Available online at www.sciencedirect.com
ScienceDirect
Polymer 48 (2007) 827–840
polymer
www.elsevier.com/locate/polymer

Polymer nanocomposites based on transition metal ion modified organoclays

Pranav Nawani [a], Priya Desai [a], Matt Lundwall [a], Mikhail Y. Gelfer [a], Benjamin S. Hsiao [a,*], Miriam Rafailovich [b], Anatoly Frenkel [c], Andy H. Tsou [d], Jeffrey W. Gilman [e], Syed Khalid [f]

[a] *Chemistry Department, Stony Brook University, Stony Brook, NY 11794-3400, United States*
[b] *Materials Science and Engineering Department, Stony Brook University, Stony Brook, NY 11794, United States*
[c] *Physics Department, Yeshiva University, New York, NY 10016, United States*
[d] *Butyl Polymers Technology, ExxonMobil Chemical Company, Baytown, TX 77522-5200, United States*
[e] *Fire Research Division, National Institute of Standards and Technology, Gaithersburg, MD 20899-8665, United States*
[f] *National Synchrotron Light Source, Brookhaven National Laboratory, Upton, NY 11973-5000, United States*

Received 12 October 2006; received in revised form 3 December 2006; accepted 4 December 2006
Available online 3 January 2007

Abstract

A unique class of nanocomposites containing organoclays modified with catalytically active transition metal ions (TMI) and ethylene vinyl acetate (EVA) copolymers was prepared. The morphology, thermal and rheological properties of these nanocomposites were studied by thermal gravimetric analysis (TGA), transmission electron microscopy (TEM), extended X-ray absorption fine structure (EXAFS) spectroscopy, X-ray scattering/diffraction and oscillatory shear rheometry. TMI-modified organoclays were thought to possess pillaring of multivalent TMI in the interlayer silicate gallery, leading to a notable reduction of the interlayer *d*-spacing. The resulting nanocomposites exhibited significantly improved thermal stability and fire retardation properties, but similar morphology (i.e., an intercalated–exfoliated structure) and rheological properties comparable with EVA nanocomposites containing unmodified organoclays. It appears that the compressed organic component in the TMI-modified organoclay can still facilitate the intercalation/exfoliation processes of polymer molecules, especially under extensive shearing conditions. The improved fire retardation in nanocomposites with TMI-modified organoclays can be attributed to enhanced carbonaceous char formation during combustion, i.e., charring promoted by the presence of catalytically active TMI.

Keywords: Transition metal ion; Organoclay; Nanocomposite

1. Introduction

Thermoplastic nanocomposites with improved barrier, mechanical, thermal, and fire retardation properties have attracted a great deal of attention from both academic and industrial laboratories in the past several years [1,2]. Polymer nanocomposites can be considered as filled materials with at least one dimension of the filler in the nanometer range. Organoclays are organically modified layered silicates, which have been widely used as nanoscale fillers [3]. As organoclays can be intercalated or exfoliated by polymer molecules, the enhancement in modulus, toughness, and barrier properties may be obtained. Typically, the improved properties can be achieved at relatively low filler loading ($\phi < 10$ wt%) in nanocomposites as compared to 30–50 wt% of fillers in conventional composites.

Although organoclays have been frequently mentioned as effective fire retardant agents, their fire retardation (FR) properties are not sufficiently high [4]. The FR activity of organoclay is usually attributed to its ability to drastically enhance the melt viscosity of filled materials, thus slowing down the diffusion of highly combustible products and promoting the

* Corresponding author. Tel.: +1 631 632 7793; fax: +1 631 632 6518.
E-mail address: bhsiao@notes.cc.sunysb.edu (B.S. Hsiao).

0032-3861/$ - see front matter © 2007 Elsevier Ltd. All rights reserved.
doi:10.1016/j.polymer.2006.12.005

formation of silica-rich carbonaceous char to starve the flame of fuel [4–7]. Charring is an important mechanism of the FR activity, yet it is not well understood. It was suggested that charring in nanocomposites could be partially attributed to their catalytic activity, facilitating processes such as oxidative dehydrogenation and aromatization [5,6,8–11]. In this study, we hypothesize that the catalytic efficiency of organoclays based on montmorillonite mineral can be improved by incorporation of common transition metal ions (TMI), such as Cu or Fe. This is because the addition of TMI complexes to polymers has been proven to enhance fire retardancy [12,13]. It appears that the presence of TMI promotes crosslinking of various polymers, enhances charring and slows down thermal degradation. On the other hand, TMI may also catalyze chain scission, thus making polymers more volatile and degradable.

Recently, we demonstrated that organoclays modified with TMI can significantly improve the thermal stability, reduce the release rate of volatile products from thermal degradation, and increase the content of solid residue upon heating at 900 °C in air [14]. These characteristics suggest that TMI-modified organoclays may also improve the fire retardation properties of corresponding nanocomposites. Currently, as the FR activity of organoclay is insufficient to replace conventional FR additives, they are often used in combination with proven FR agents such as hydrated alumina ($Al_2O_3 \cdot H_2O$) or carbon nanotubes [15–17]. Insufficient FR activity of organoclays can be attributed to thermal degradation of surfactant components via Hoffman elimination [18], resulting in the emission of combustible volatile products. We hypothesize that the TMI-modified organoclays can at least partially overcome this problem.

The overall purpose of this work was to determine the effect of TMI-modified organoclays on structure, rheology, thermal stability and fire retardation properties of EVA-based nanocomposites. For this purpose, small-angle X-ray scattering (SAXS), scanning and transmission electron microscopies (SEM/TEM), thermal gravimetric analysis (TGA) and extended X-ray absorption fine structure (EXAFS) spectroscopy, rheological and fire testing techniques were used. The specific goal of this study was to verify the effect of catalytically active TMI on the thermal stability of EVA/organoclay nanocomposites. We suggest that the TMI modification of organoclays, taking advantage of the unique surface chemistry and adsorption capacity of organoclays, may lead to effective fire retardant materials. In particular, we expect TMI-modified organoclays to have dual physico-chemical mechanisms of fire retardancy [14]. In the physical mechanism, organoclays can act as barriers for gas diffusion and physical crosslinks that hamper the flow of polymer melt, resulting in flammability reduction [1,2,4–6]. In the chemical mechanism, TMI-modified organoclays can promote a variety of reactions during combustion, thus facilitating the formation of carbonaceous char. These reactions may include oxidative dehydrogenation, olefin dimerization and aromatization [8–11]. In addition, we demonstrate that TMI-modified organoclays can remain compatible with the polymer matrix, similar to unmodified organoclays. This is usually not the case for conventional FR agents.

Two TMI systems based on Fe and Cu salts were selected to modify a commercially available organoclay (C20A). The chosen polymer system was ethylene vinyl acetate (EVA) copolymer. We have recently studied the miscibility, rheology and morphology of EVA/C20A nanocomposites [19], which can be viewed as a good model system for comparison of nanocomposites containing TMI-modified organoclays. The motivation for the selection of Cu^{2+} and Fe^{3+} TMI is as follows. (a) As Cu^{2+} compounds have been extensively demonstrated as effective FR agents and smoke suppressants [20], one may expect that the FR activity of Cu-modified organoclays can be improved. (b) The literature data suggest that the FR activity of Cloisite-based organoclays may be partially due to the presence of iron [21], through the formation of iron oxides during thermal degradation. Thus, Fe-modified organoclays and the corresponding nanocomposites were also investigated in this study.

2. Experimental

2.1. Materials and preparation

The organoclay sample (Cloisite® 20A or C20A) used in this study was manufactured by the Southern Clay Company. Based on the data provided by Southern Clay, C20A contained montmorillonite mineral clay (Wyoming Cloisite) and dimethyl di-hydrogenated tallow ammonium chloride (DMDTA) surfactant. The content of the surfactant in C20A was 35 wt%. DMDTA is a blend of surfactants by Akzo Nobel. The major component in this blend is di-methyl di-octadecyl ammonium chloride (DMDOA); minor components included (in the order of decreasing content) di-methyl octadecylhexadecyl ammonium chloride, di-methyl di-hexadecyl ammonium chloride, and a small amount (<3 wt%) of tertiary ammonium chlorides (such as di-methyl octadecyl ammonium chloride and di-methyl-hexadecyl ammonium chloride). Solvents and transition metal salts used in this study were purchased from Aldrich Chemicals. These salts were acquired in their hydrated forms as $CuCl_2 \cdot 2H_2O$ and $FeCl_3 \cdot 6H_2O$. The polymer used for making the nanocomposite was ethylene vinyl acetate (EVA was a member of Elvax® by DuPont Company). The polymer contained 8 mol% of vinyl acetate, its molecular weight (M_w) was 110 kg/mol and the polydispersity was $M_w/M_n \sim 6.0$. It had an LDPE-like structure, i.e., containing long chain branches.

Modified organoclays were prepared by treating the organoclay suspensions in alcohol (ethanol or methanol) with a TMI solution in the same solvent. The general preparation procedures were described below. Organoclay samples were thoroughly washed before the TMI treatment. The washing step was necessary to remove excess surfactants in organoclay. The typical washing procedures were as follows. Clay sample (organoclay, 2 g) was placed in 40 ml of solvent (methanol). The pH value for each organoclay suspension was maintained above 7 for cationic exchange to take place. The organoclay suspension was vigorously stirred for 24 h. Upon stirring for few hours, the dispersion turned into a viscous slurry due to the swelling of the clay. The slurry was then filtered and dried

in vacuum for 12 h at 80 °C (the weight loss observed for each washed organoclay sample was negligible). The washed and dried samples were then placed in appropriate TMI solutions (0.30 M, using the same solvent as in the washing process) for ion exchange. The clay suspension was kept in a closed container to prevent solvent evaporation under vigorous stirring for 36 h. After the TMI treatment, the samples were filtered, washed again and dried in vacuum for 12 h at 80 °C. For TMI-treated organoclay, after the washing step, the recovered solvent was checked for chloride ions using 0.1 N $AgNO_3$. The washing step was repeated several times until there was no precipitate formation upon the addition of $AgNO_3$, which ensured the absence of unbound surfactants.

Nanocomposites were prepared by melt blending of EVA copolymer with unmodified organoclays or TMI-modified organoclays using a microprocessor (DACA, US). The combined weight of TMI-modified organoclay and polymer was 3.0 g/load. Mixing was performed at 170 °C at 200 rpm under the flow of nitrogen. The mixing time was 10 min unless specified otherwise. After mixing, the polymer nanocomposite was extruded and subsequently pressed by a carver pressing apparatus at 170 °C and 4000 psi pressure. Samples were left for annealing for 30 min and were allowed to cool down to room temperature. Typical size of polymer nanocomposite film made for X-ray measurements was 4 mm × 4 mm with 1 mm thickness.

2.2. Sample characterization

2.2.1. Synchrotron X-ray scattering and diffraction

Simultaneous SAXS (small-angle X-ray scattering) and WAXD (wide-angle X-ray diffraction) measurements were performed using two 1D linear position sensitive detectors (EBML, Grenoble, France) at the X27C beamline in the National Synchrotron Light Source (NSLS), Brookhaven National Laboratory (BNL). The wavelength of the X-ray was 1.366 Å. Silver behenate was used to calibrate the scattering angle in SAXS and aluminum oxide was used to calibrate the diffraction angle in WAXD. X-ray measurements for all TMI-modified organoclays and nanocomposite samples were taken under the same conditions. In situ high temperature X-ray measurements were carried out in a custom-made environmental chamber, where the maximum temperature was around 350 °C.

2.2.2. 2D and 3D transmission electron microscopy

All nanocomposite samples were cryo-microtomed at −150 °C using a diamond knife to obtain sections of 100 nm thickness for transmission electron microscopic (TEM) characterization. No staining was applied. 2D TEM images were acquired on a JEOL 2000FX TEM instrument at 160 kV accelerating voltage. Multiple images from various locations at different magnifications were collected to provide an overall assessment of dispersion uniformity. For 3D TEM, the FEI Tecnai TEM instrument (G2 F20 Super Twin TMP) was used. All samples were run on the scanning transmission electron microscopy high-angle annular dark field (STEM-HAADF) mode to minimize the sample damage, while maximizing the contrast. The image acquired in such a way is also known as STEM-HAADF tomography. During the measurement, the sample was tilted from a 0° to −60°, which took about 90 min, and the samples were tilted back from 0° to 60°, which took another 90 min. The total exposure time was 3 h. The images were reconstructed using the Voltex 3D volume rendering software.

2.2.3. Extended X-ray absorption fine structure spectroscopy

Extended X-ray absorption fine structure (EXAFS) spectroscopic measurements were performed to determine the oxidation states of metal ions in the TMI-modified organoclays using a PIPS detector at beamline X18B in the NSLS, BNL. Copper and iron foils were used as calibration standards for the EXAFS data interpretation. In this experiment, a Si(111) channel cut monochromator was used for data collection. The beam size was 10 mm × 1 mm. The energy resolution, corresponding to the vertical opening, was approximately 1 eV at the copper edge. The monochromator was positioned at 18 m from the source and the samples were placed inside the hutch, 2 m downstream from the monochromator. This is an unfocused beamline with a photon flux of 2×10^{10} photons/s at the copper edge. Sealed ion chambers (30 cm long) from Oxford-Danfysik Instruments were used for the determination of the incident intensity (I_0) and the transmission intensity (I_t). The PIPS detector (Canberra) was used to collect the fluorescence data. The I_0 detector was filled with 50% He and 50% N_2, and I_t with 90% N_2 and 10% Ar, all at the atmospheric pressure. The sample or the reference foil was placed between the I_t and I_{ref} (sample chamber) ion chambers, where flowing N_2 was used in the sample chambers. In a typical measurement, the monochromator was detuned to 30% at the iron edge to minimize higher harmonics. All detectors were checked for linearity and the offsets were taken into account to eliminate the electronic noise.

2.2.4. Rheological measurements

Rheological measurements were performed using a Physica MCR301 rheometer (Anton Paar Inc., Austria) to determine the viscoelastic behavior of nanocomposites in the molten state. A 25 mm parallel plate fixture was used and a constant strain amplitude ($\gamma = 0.06$) was applied in all dynamic measurements. The frequency scan ($0.1 < \omega < 100$ rad/s) for acquisition of oscillatory shear data was repeated 4 times at each temperature. Isothermal rheological properties such as storage (G') and loss (G'') moduli were determined, which were very much reproducible in each run. All measurements were performed in the controlled strain regime under the flow of nitrogen to avoid thermal decomposition.

2.2.5. Thermal gravimetric analysis

Thermal gravimetric analysis (TGA) measurements were performed using a TA 7 thermal analyzer, manufactured by Perkin–Elmer. All measurements were carried out in the temperature range of 40–800 °C and at a heating rate of 20 °C/min. TGA data collection for all nanocomposite samples was taken under identical conditions.

2.2.6. Flame test

Extruded cylindrical rods (2 mm diameter; 100 mm long) of polymer nanocomposites were ignited for 5 s and were allowed to burn in air, whereby the char was collected afterwards. The experimental setup closely resembled that of the standard UL94 test [22] with the exception that thinner samples were used in order to reduce the amount of nanocomposite tested. The ignition and burning examinations of nanocomposites were carried out in an environment without air drift and the flame was calibrated according to the UL94 procedures. Five samples were burnt according to UL94 test description [22] for each of polymer nanocomposite samples and these results are averaged to determine the rate of burning.

3. Results and discussion

3.1. SAXS/WAXD to determine the structure of nanocomposites

In a publication described elsewhere [14], the TMI modification was shown to have a profound effect on the *d*-spacing of organoclay. The amount of TMI in modified clays is shown in Table 1. The measured values of *d*-spacing for organoclays and TMI-modified organoclays in this study are listed in Table 2. It is seen that the *d*-spacing values for Fe- and Cu-modified organoclays (prepared in methanol) were notably smaller (*d*-spacing = 2.32 nm for Cu-modified C20A and 1.40 nm for Fe-modified C20A) than that of unmodified C20A (2.56 nm). However, these values are still larger than that of pristine montmorillonite clay (*d*-spacing = 1.28 nm). This suggests that TMI penetrated into the gallery of organoclay, resulting in the collapse of intercalated layers. The argument that TMI were predominantly confined in the interlayer space rather than deposited on the surface of clay particles was further verified by SEM and WAXD techniques and elemental analysis [14]. From the above results, it appears that TMI can form pillar-like aggregates in the interlayer gallery of the organoclays, whereby the structure enhances the binding of neighboring clay layers and decreases the *d*-spacing. This notion has raised the following concern. Since some ''weak'' surfactant molecules are replaced by TMI, the modification process seems to impose an adverse effect on the resulting nanocomposite, i.e., the reduced concentration of surfactant molecules may hinder the intercalation and exfoliation of polymer molecules. To verify this concern, simultaneous SAXS and WAXD measurements on nanocomposites based on TMI-modified organoclays were carried out and the results are described as follows.

Table 1
Elemental analysis results for unmodified C20A and TMI-modified C20A

Material analyzed	C20A	C20A washed	C20A Cu	C20A Fe
Carbon	28.9	27.23	23.13	25.11
Hydrogen	6.02	5.53	4.92	5.2
Nitrogen	0.89	0.84	0.79	0.84
Copper	0.0	0.0	3.42	0.0
Iron	1.74	1.56	0.94	4.13
Chloride	0.01	0.01	3.5	0.1

Table 2
The *d*-spacing values of unmodified C20A and TMI-modified C20A

Sample	Montmorillonite clay	Unmodified C20A	Cu-modified C20A	Fe-modified C20A
d-Spacing (nm)	1.28	2.56	2.32	1.40

Fig. 1a shows SAXS profiles of various nanocomposites (EVA/C20A and EVA/TMI-modified C20A) prepared by melt mixing for 10 min. In EVA/C20A nanocomposites, the scattering peak at 0.24 nm^{-1} (*d*-spacing = 4.16 nm) represents the intercalated structure induced by EVA chains, since the *d*-spacing of C20A is only 2.56 nm (Table 2). However, it is interesting to note that all three profiles in Fig. 1a (EVA/C20A, EVA/Cu-modified C20A and EVA/Fe-modified C20A) exhibit similar scattering features (i.e., similar peak shape and position), suggesting a nearly identical layered structure. These results indicate that the intercalation of TMI-modified organoclays by EVA chains took place, just like in the system of unmodified organoclays. Broadening of SAXS peaks was found in the scattering profiles of all nanocomposites, indicating that the average stack size was decreased due to partial delamination of organoclays. The above results verify that there is a reasonable compatibility between TMI-modified organoclays and the EVA matrix. The corresponding WAXD profiles of various nanocomposites (EVA/C20A and EVA/TMI-modified C20A) are shown in Fig. 1b, which also exhibit similar diffraction features mainly from the clay structure. No crystal structure from the Cu or Fe phase was observed, confirming that no large Fe or Cu crystals were formed. This is consistent with the notion that TMI have penetrated into the gallery of organoclay.

Fig. 1c shows that shorter shearing time (3 min) in melt mixing led to an intermediate layered structure with relatively sharp SAXS peaks positioned in-between those in organoclays (or TMI-modified organoclays) and corresponding nanocomposites. This suggests that inefficient delamination of clay stacks (i.e., intercalation) took place in the matrix. It is evident that the pillaring effect of TMI on the collapse of the layered structure, while notable in the pure filler form, can be overcome by sufficient shearing. All the following results were obtained from shearing for 10 min since longer time shearing did not affect the layer structure in TMI-modified clays. In addition, as we did not observe a noticeable change in the structure of the nanocomposites when the weight percentage of clay is increased from 5 to 10 wt% (Fig. 1d), all the following results were also obtained using 10 wt% of nanofillers unless specified otherwise. The temperature dependence of nanostructure in nanocomposites was investigated using in situ SAXS techniques. Our previous results indicate that the *d*-spacing in EVA/C20A nanocomposites always decreases with temperature, which can be attributed to the reduced compatibility between polymers and organoclays (i.e., the LCST-like phase behavior) [19]. It is seen that as temperature is increased from 80 to 200 °C, the SAXS peaks in EVA/C20A (Fig. 2a), EVA/Cu-modified C20A (Fig. 2b) and

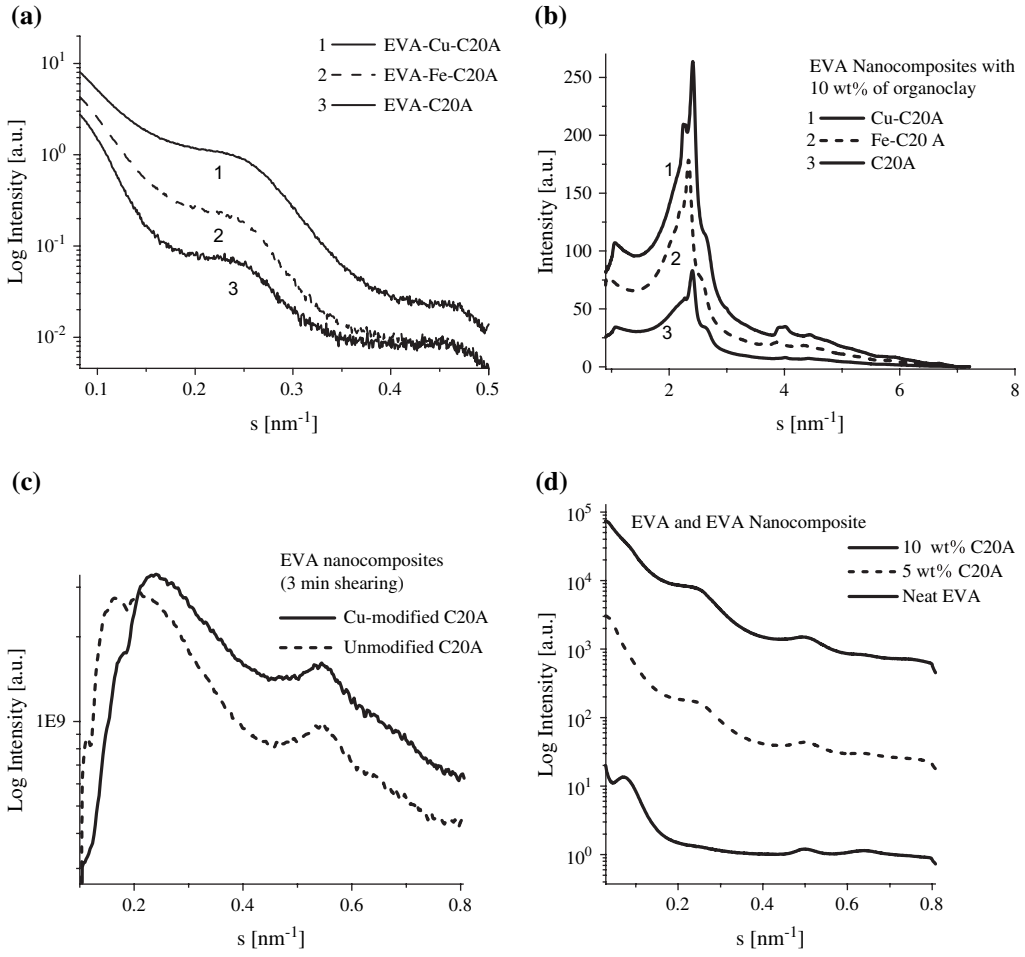

Fig. 1. (a) SAXS profile of EVA/C20A and EVA/TMI-modified C20A mixed for 10 min. (b) WAXD profiles of EVA/C20A and EVA/TMI-modified C20A mixed for 10 min. (c) SAXS profile of EVA/C20A and EVA/Cu-modified C20A mixed for 3 min. (d) SAXS profile of EVA/C20A containing various percentages of unmodified C20A.

EVA/Fe-modified C20A (Fig. 2c) all shifted towards higher s values (i.e., the d-spacing decreased). The d-spacing values of various nanocomposites at different temperatures are listed in Table 3. From these results, it appears that EVA/TMI-modified C20A nanocomposites also exhibited the LCST-like polymer–clay phase segregation behavior [19]. Several interesting features were noted from the above results. (1) The loss of peak features in SAXS profiles after the heating–cooling cycle was less pronounced in EVA/TMI-modified C20A than that in EVA/C20A. (2) The broadening of SAXS peaks during heating cycle within the temperature range of 120–280 °C and subsequent cooling cycle was more significant for a system containing non-modified organoclay than in its TMI-modified analogs. (3) In EVA/C20A, after the heating–cooling cycle, SAXS peaks drastically broadened and the maximal positions did not recover upon cooling to 30 °C. Previously, the loss of scattering features in SAXS for EVA/C20A at temperatures above 200 °C was attributed to thermal degradation of organic surfactants in organoclays [23]. The above results confirm that EVA/C20A nanocomposites, containing unmodified or TMI-modified C20A, can undergo thermally reversible phase segregation upon heating above 180 °C, resulting in de-intercalation of organoclays and decrease of the average d-spacing. However, as the temperature decreases, the compatibility between organoclay and EVA increases, which results in only partial re-intercalation of clay layers by EVA [19]. This can be explained by the surfactant loss during the heating cycle that leads to the loss of periodicity during re-intercalation, thus the original structure cannot be recovered completely. This process can also explain the weakening of scattering features in SAXS. At high temperatures, further desorption and degradation of the surfactant component may cause the complete collapse of organic layers. The resulting loss of periodicity in the layer structure can cause the shift and broadening of SAXS peaks, as observed in the chosen EVA8-C20A (with and without TMI modification) systems as well as in montmorillonite-based organoclays undergoing heating in the absence of polymers [19,23].

The persistence of SAXS features in EVA/TMI-modified C20A nanocomposites (Fig. 2) indicates that TMI-modified organoclays have higher thermal stability than unmodified organoclays. This was further supported by the following observations. (1) Only moderate broadening of SAXS peaks was observed in TMI-modified systems, (2) after the heating–cooling

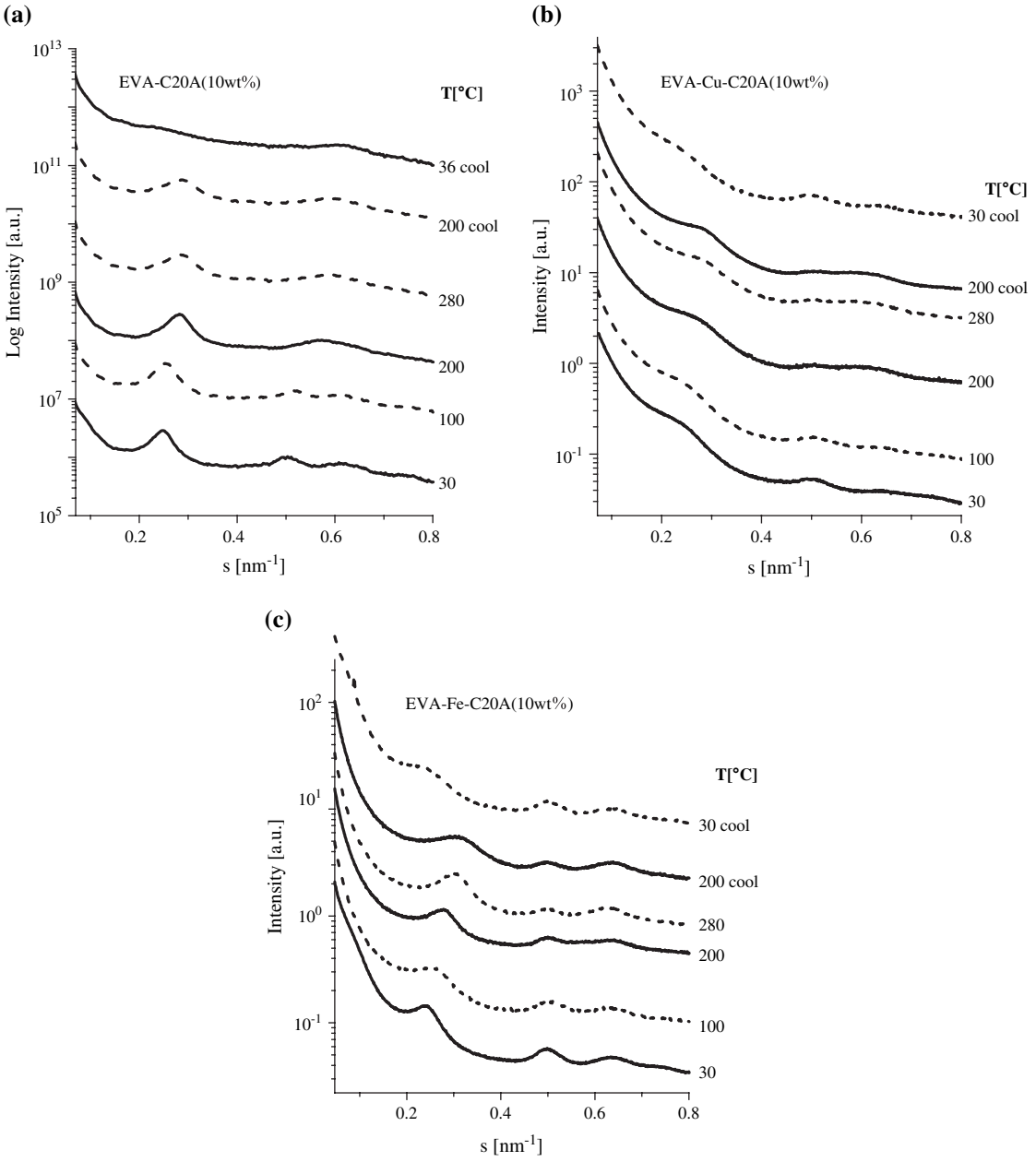

Fig. 2. Temperature resolved SAXS profile for EVA organoclay nanocomposites in a heating–cooling cycle: (a) EVA nanocomposites containing unmodified C20A, (b) EVA nanocomposites containing Cu-modified C20A, and (c) EVA nanocomposites containing Fe-modified C20A.

cycle, positions of SAXS peaks mostly recovered. For example, the SAXS profile from EVA/Cu-modified C20A showed that scattering peaks moderately broadened and weakened at temperatures above 200 °C (albeit to a lesser degree than in the EVA/C20A nanocomposite). However, in EVA/Fe-modified nanocomposites, these peak features remained almost unchanged, i.e., all peaks were sharp during the heating–cooling cycle. We hypothesize that the pillaring of organoclays by TMI does not allow for the complete collapse of organic layers, even when surfactant loss is significant. In addition, TMI were shown to increase the thermal stability of organoclays and reduce loss of organic component via formation of volatile products, thus preserving the periodical structure of layered systems during heating–cooling cycle. This suggests that even higher structure stability at high temperatures (<260 °C) can be achieved in an EVA/Fe-modified C20A system as compared to that in EVA/Cu-modified C20A.

Table 3
The *d*-spacing value in EVA nanocomposites containing unmodified C20A and TMI-modified C20A at different temperatures

Temp. (°C)	*d*-Spacing (nm) of neat C20A	*d*-Spacing (nm) of Cu-modified C20A	*d*-Spacing (nm) of Fe-modified C20A
30	4.16	3.97	4.13
100	4.01	3.96	4.13
200	3.60	3.69	3.70
280	3.51	3.27	3.59
200 °C cooling	3.54	5.29	3.56
30 °C cooling	4.26	4.40	4.53

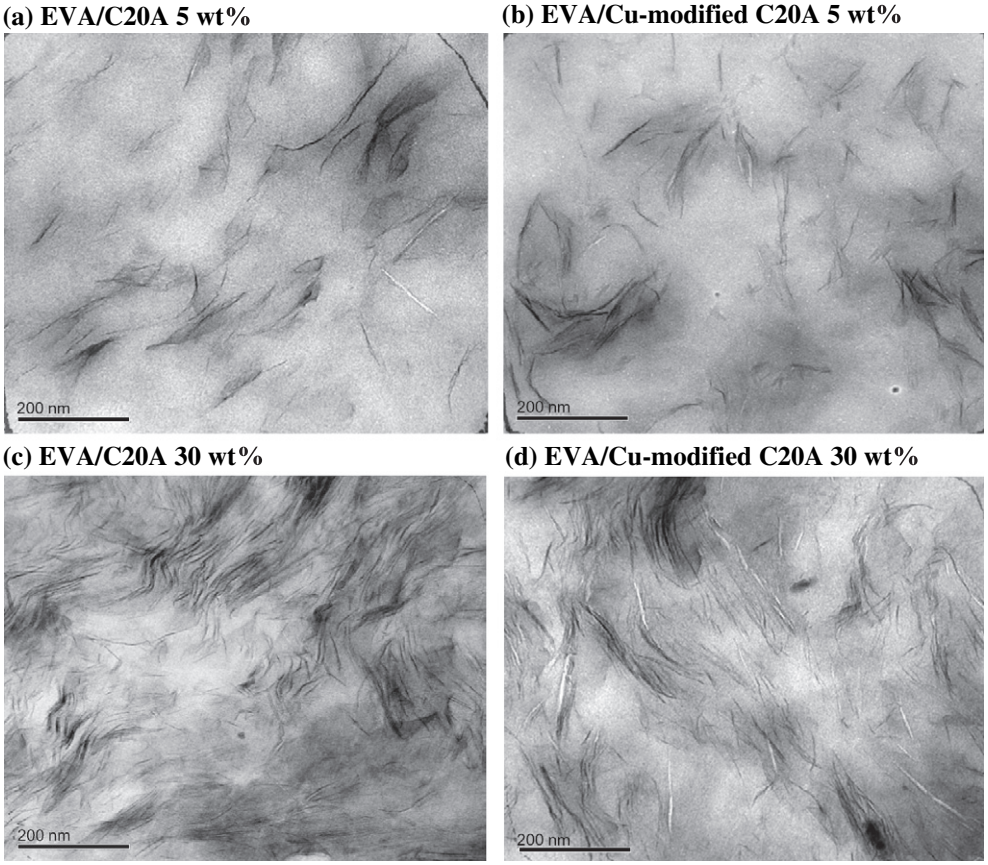

Fig. 3. 2D TEM images of EVA nanocomposites containing various weight percentages of organoclays: (a) 5 wt% of unmodified C20A, (b) 5 wt% of Cu-modified C20A, (c) 30 wt% of unmodified C20A, and (d) 30 wt% of Cu-modified C20A.

3.2. TEM examination of TMI-modified clay morphology

TEM micrographs of EVA/organoclay (with and without TMI modification) nanocomposites are shown in Fig. 3. Excellent spatial resolution with a clear definition of the layered structure in intercalated C20A could be seen in these micrographs. Fig. 4 shows the 3D TEM image of cryo-microtomed EVA/C20A (10 wt%) nanocomposite samples with the thickness of about 100 nm. The examined 3D volume was $1.6 \times 1.6 \times 0.1\ \mu m^3$. The 3D TEM view of extracted clay phase provides a good estimate of the dispersion state of organoclays in the bulk sample. It is clear that the clay stacks were not completely exfoliated in these nanocomposites, which is in accordance with the SAXS data indicating the existence of the intercalated–exfoliated structure. In Fig. 3a and b, 2D TEM micrographs of EVA containing 5 wt% C20A and 5 wt% of Cu-modified C20A were compared. Both systems exhibited a similar intercalated–exfoliated structure. With C20A loading increased to 30 wt%, strong local planar orientations in some locations were seen, which were also observed in the 3D view (Fig. 4). Based on the 2D images from EVA/Cu-modified C20A (which was also the case of EVA/Fe-modified C20A, data not shown), we again verified that there were no aggregates of TMI crystals in EVA/TMI-modified C20A nanocomposites.

3.3. EXAFS to investigate the oxidation state of TMI in modified organoclays

Polymer nanocomposites containing Cu- and Fe-modified C20A organoclays were investigated by EXAFS to determine the oxidation state of TMI, which was essential for the catalytic activity that could improve the FR properties. Results from the EVA/Cu-modified C20A nanocomposites showed that the Cu edge was slightly shifted towards a lower energy value than that of the Cu^{2+} standard. The Cu K-edge EXAFS (or X-ray absorption near edge structure, XANES) profile indicated that Cu appeared predominantly in the +1 oxidation state (Fig. 5a). In addition, the Cu K-edge EXAFS profile indicates the absence of elemental Cu. Due to the heterogeneity of the sample, it is not possible to state unambiguously which Cu complex is present. The theoretical K-edge value for Cu is 8979 eV and for Cu^{2+} is 8990 eV. The K-edge value for organoclays modified with copper was found to be between 8979 and 8990 eV (more towards 8990 eV). This suggests that in EVA/Cu-modified C20A nanocomposites, the adsorbed copper is not Cu^{2+} but probably in a mixed state [14]. In other words, it is more likely that the adsorbed copper is in more than one form, i.e., partial reduction of Cu^{2+} to Cu^{1+} may take place.

In our previous study [14], we showed that the oxidation state of Fe in Fe-modified C20A was very close to that of

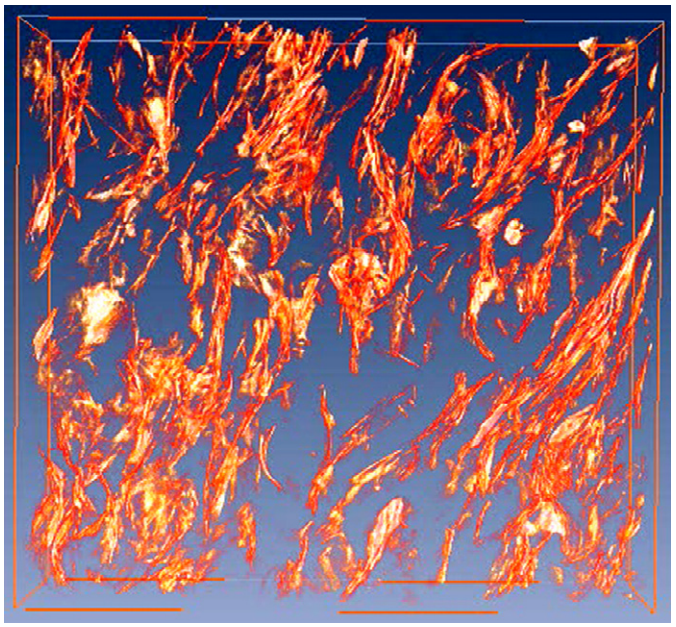

Fig. 4. 3D TEM images of EVA nanocomposites containing 10 wt% of unmodified C20A.

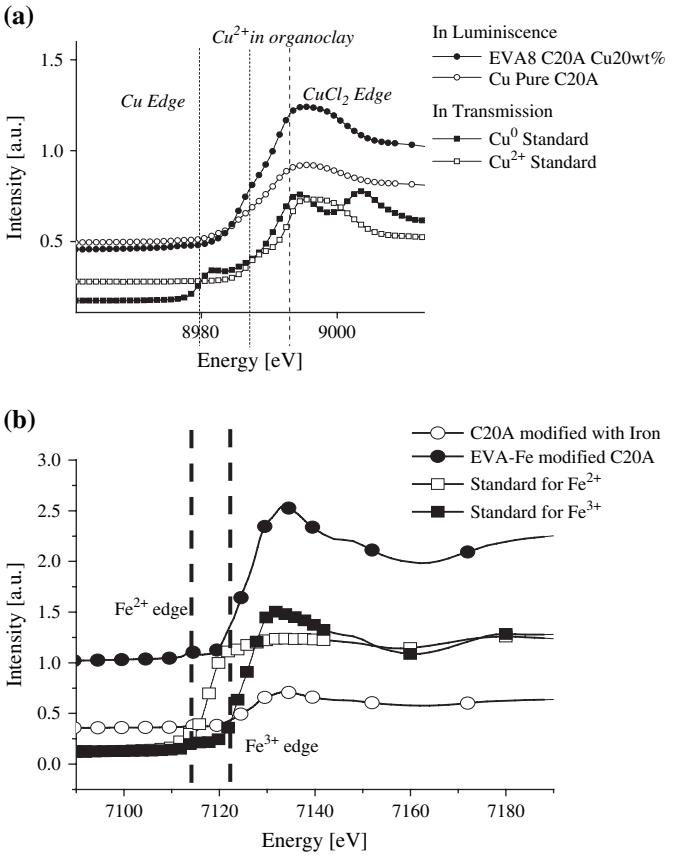

Fig. 5. EXAFS profile for EVA nanocomposite containing TMI-modified C20A and the reference materials: (a) EXAFS profile of Cu and Cu^{2+}, results indicate the presence of Cu^{1+} and Cu^{2+} in the EVA and Cu-modified C20A nanocomposites. (b) EXAFS profile of Fe and Fe^{3+}, results indicate the presence of Fe and Fe^{3+} in the EVA and Fe-modified C20A nanocomposites.

Fe^{3+} and was thermally stable. Fig. 5b illustrates Fe K-edge EXAFS profiles of EVA/Fe-modified C20A nanocomposite and Fe^{3+} standard. Although the EVA/Fe-modified C20A nanocomposite also exhibited the high degree of oxidation state for Fe, there were some differences between the oxidation state of Fe-modified C20A and that of corresponding nanocomposites. It appeared that Fe was in different oxidation states in the EVA/Fe-modified C20A nanocomposite, i.e., a mixed state of Fe^{3+}, Fe^{2+} and Fe^0. The reason for the reduction mechanism of Fe^{3+} to Fe^{2+} and to Fe^0 is still not clear and will be the subject of a future study. Residual solvent, methanol can be responsible for reduction of TMI in the organoclays but we doubt that there could be any effect on oxidation state of TMI during the processing of nanocomposites.

It has been shown that the presence of Cu promotes crosslinking of the polymer matrix (PVC) during combustion [20]. Although the choice of polymer is different (EVA) here, we expect a similar behavior to take place, i.e., the crosslinking reaction will occur in the presence of TMI. It was suggested that the state of Cu(I), irrespective of the state of oxidation, exhibited better burning efficiency (thus better flame retarding properties as less volatile combustible products are produced) than Cu(II) and Cu(0), which also improve the fire retardation but in a lesser degree. Our results generally support this conclusion.

3.4. Rheological characterization of nanocomposites

It has been shown by us earlier that the introduction of C20A into the EVA matrix would result in physical gelation of EVA [19,24], whereas the rheological behavior of pure EVA is typical of linear polymer melts. The thermo-rheological responses of storage modulus (G'), loss modulus (G'') and dynamic viscosity (η) for EVA and EVA/organoclay nanocomposites with unmodified C20A and TMI (Cu and Fe)-modified C20A are shown in Figs. 6–8, respectively. The rheological behavior of pure EVA was consistent with our previous publications. In brief, the EVA melt followed the time–temperature superposition (TTS) principle, where the slope in $G'(\omega)$ curve in the terminal zone (low frequency) was close to 2 (Fig. 6a) and that in $G''(\omega)$ was close to 1 (Fig. 7a). The frequency dependence of the dynamic viscosity $\eta^*(\omega)$ exhibited a Newtonian region at low frequencies and a power-law region at higher frequencies (Fig. 8a). Furthermore, the viscoelastic parameters of EVA (i.e., G', G'' and η^*) strongly depended on the temperature, and their magnitudes decreased upon heating, which could be described by the Arrhenius law.

In contrast, the EVA/C20A nanocomposite exhibited the pseudo-solid rheological behavior [19]. In this nanocomposite, the Newtonian region in $\eta^*(\omega)$ was absent and the viscoelastic response followed a power-law relation with frequency throughout the tested range (Fig. 8b). The most notable feature of thermo-rheological behavior of EVA/C20A nanocomposites was the sharp deviation from the TTS principle, whereby the temperature dependence of viscoelastic functions was very weak. For example, the value of η^* at 0.1 rad/s in pure EVA decreased to three orders of magnitude when temperature

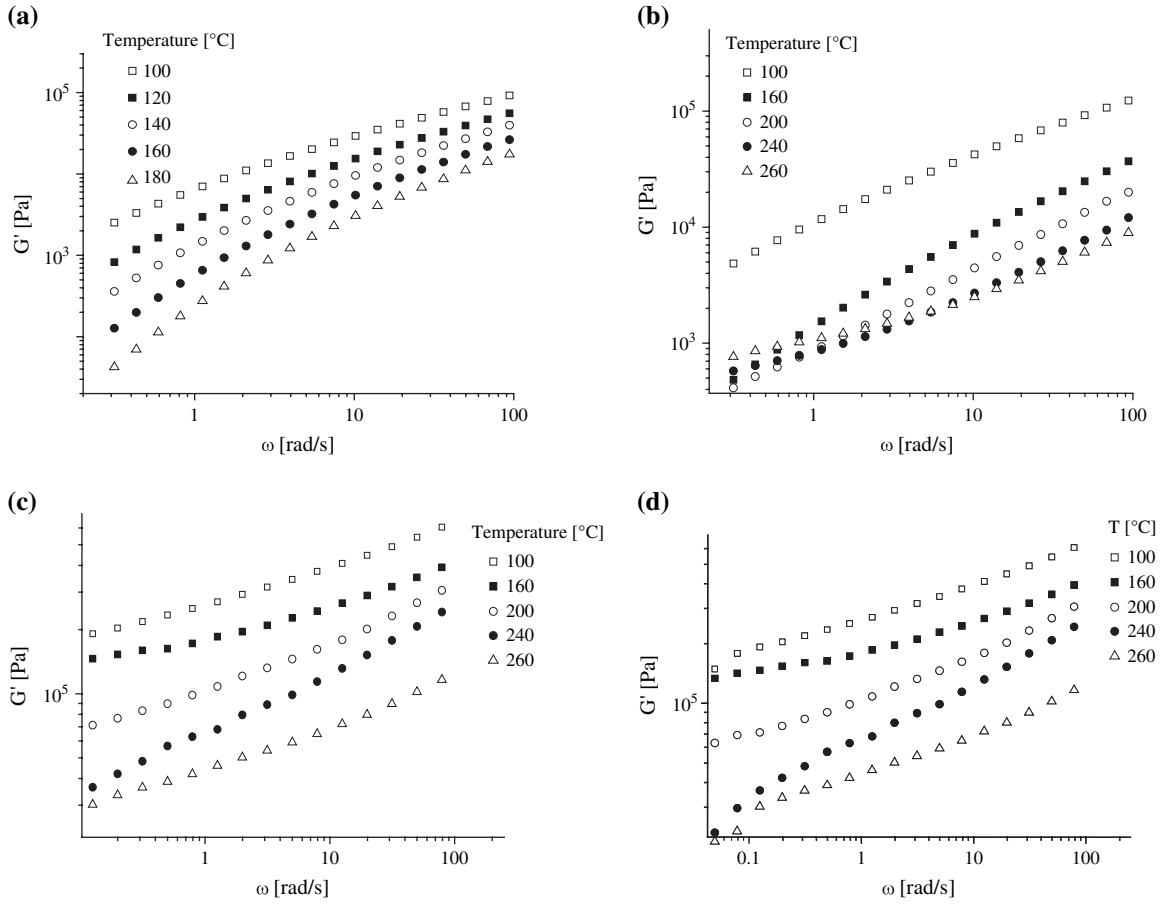

Fig. 6. Temperature dependence of storage modulus (G') for EVA and EVA/organoclay nanocomposites with unmodified C20A and TMI (Cu and Fe)-modified C20A: (a) neat EVA, (b) EVA/C20A, (c) EVA/Cu-modified C20A, and (d) EVA/Fe-modified C20A.

increased from 110 to 200 °C, whereas the corresponding decrease in the same temperature range was only 30% in the EVA/C20A nanocomposite (Fig. 8b). The weak temperature dependence of viscoelastic properties could be beneficial for the FR performance of nanocomposites. It has been well documented that burning polymers (e.g., EVA) can easily spread the fire due to the low melt viscosity. The physical gelation characteristics of nanocomposite melt would hinder the flow properties, thus retarding the fire spread.

Fig. 6a shows the $G'(\omega)$ vs. ω profile of molten EVA. The slope of $G'(\omega)$ was less than 2, higher than that of $G''(\omega)$, which was less than 1. This behavior is typical of linear polymer melts with the characteristics of a single Maxwell component. One can argue that the terminal domain of EVA, positioning at frequencies below 0.1 rad/s, can be experimentally obtained. In contrast, in the presence of organoclay (modified and unmodified in Fig. 6b–d), the appearance of a plateau region at low frequencies in $G'(\omega)$ was seen. In this case, the slope of $G'(\omega)$ became less than that of $G''(\omega)$. The plateau region in $G'(\omega)$ was more pronounced at higher temperatures, which is consistent with the occurrence of physical gelation [19]. Another interesting feature in nanocomposites was the relatively weak temperature dependence of viscoelastic responses compared to that of polymer melts, which could also be explained by the thermally induced physical gelation behavior.

In our previous study [19], we have shown that the introduction of organoclays imposed a strong effect on the rheological properties of EVA, even though the EVA/montmorillonite blend formed only a mixed intercalated–exfoliated state. The miscibility between EVA and organoclays decreased as temperature increased in the range 120–240 °C because the EVA/organoclay system had a tendency to undergo phase segregation at elevated temperatures (due to the escape of surfactant in organoclays). The occurrence of phase segregation would result in the formation of a network of clay tactoids in the polymer matrix, which could lead to thermally induced physical gelation. As a result, the EVA/C20A nanocomposite system exhibited the Bingham-like rheological behavior, which manifested itself by divergence of zero-shear viscosity and power-law character in the $\eta^*(\omega)$ profile over the entire range of experimentally observed frequency ω. Due to the formation of a tactoid network, the rheology of EVA/C20A nanocomposites was determined by the viscoelastic properties of organomineral aggregates rather than by the relaxation behavior of a polymer matrix. Thus, the temperature dependence of viscoelastic properties in EVA/C20A was rather weak as compared to unfilled EVA. The above phenomena were more pronounced at higher temperatures ($T > 180$ °C) and higher organoclay loads $\phi > 5$ wt%.

The EVA nanocomposites containing TMI-modified C20A generally showed the similar viscoelastic behavior as that of

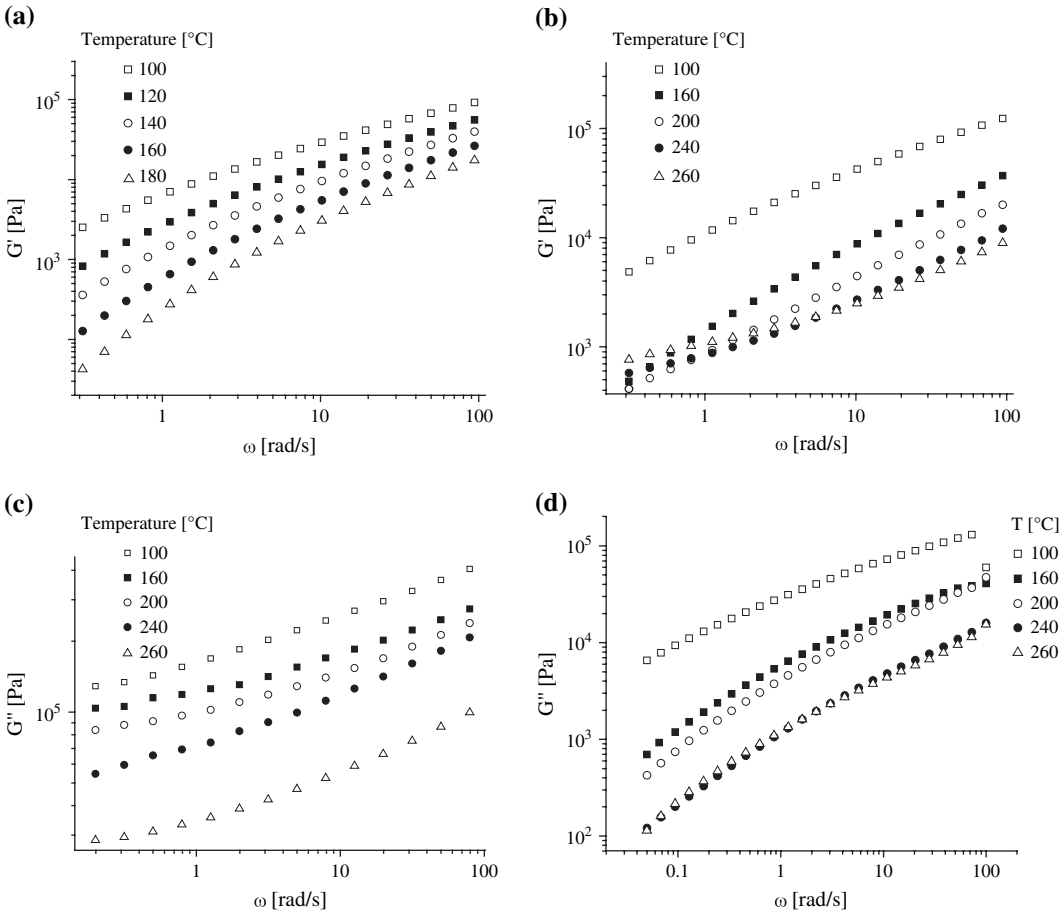

Fig. 7. Temperature dependence of loss modulus (G'') for EVA and EVA/organoclay nanocomposites with unmodified C20A and TMI (Cu and Fe)-modified C20A: (a) neat EVA, (b) EVA/C20A, (c) EVA/Cu-modified C20A, and (d) EVA/Fe-modified C20A.

EVA/C20A. For example, both EVA/Cu-modified C20A and EVA/Fe-modified C20A also exhibited weak temperature dependence of viscoelastic properties and the power-law behavior of the $\eta^*(\omega)$ curve throughout the whole range of tested frequencies (Fig. 8c and d). Although both EVA/TMI-modified C20A nanocomposites exhibited the pseudo-solid rheological behavior, when compared to that of EVA/C20A, the G' and G'' values of EVA/TMI-modified C20A systems were relatively low (Figs. 6 and 7).

Based on our previous works [19,23] as well as the TGA results in this study, it is apparent that a fraction of surfactant is permanently lost at elevated temperatures. This loss was significantly less than the overall surfactant content (40 wt%). The thermally reversible intercalation process in organoclay-based nanocomposites has been discussed previously and will not be repeated here [19]. We argue that the reason for the decrease in miscibility between polymer and organoclay at high temperatures is mainly due to desorption of some surfactant molecules from the organoclays. However, a faction of these surfactant molecules can be reabsorbed by the mineral surface upon cooling, resulting in the partial recovery of the intercalated structure. The presence of TMI can cause pillaring of the mineral phase in the gallery, which slightly decreases the extent of clay exfoliation in EVA after melt mixing. However, we believe that modification of clay surface by TMI does not make it less compatible with polymers as compared to unmodified organoclays. Thermally reversible intercalation was observed in nanocomposites containing both TMI-modified and unmodified organoclays.

Due to pillaring of clay, there is a reduction in the amount of tactoids available to the formation of tactoid networks. In Fig. 8, it is seen that the phenomena related to the formation of a tactoid network (such as power-law rheology and weak temperature dependence of η^*) were notable in the whole range of tested temperatures and frequencies in Cu-modified systems as well as in composites containing non-modified organoclays (Fig. 8b and c). In contrast, EVA containing Fe-modified organoclays (Fig. 8d) showed relatively weak temperature dependence of η^*, only at highest temperatures (above 200 °C). We hypothesize that more efficient pillaring and stronger binding of clay layers by Fe ions (carrying higher charge as suggested by EXAFS) caused the decrease in exfoliation efficiency as compared to EVA nanocomposites containing non-modified and Cu-modified organoclays. This hypothesis is consistent with the observation of sharper SAXS peaks in Fe-modified systems, which implies the existence of larger clay stacks or less exfoliation. This further suggests that the gelation behavior in EVA/TMI-modified

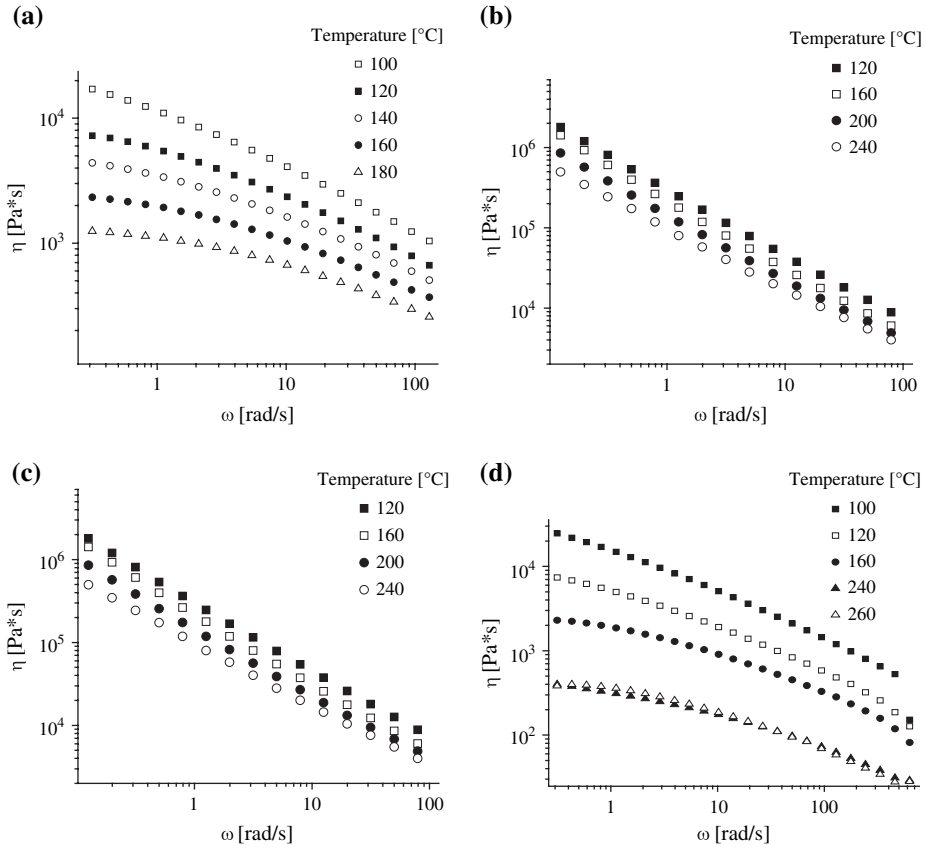

Fig. 8. Temperature dependence of dynamic viscosity (η) for EVA and EVA/organoclay nanocomposites with unmodified C20A and TMI (Cu and Fe)-modified C20A: (a) neat EVA, (b) EVA/C20A, (c) EVA/Cu-modified C20A, and (d) EVA/Fe-modified C20A.

C20A systems was less efficient than that in EVA/C20A. In fact, the rheological behavior of EVA/Cu-modified C20A was closer to that of EVA/C20A, and the rheological behavior of EVA/Fe-modified C20A was closer to that of pure EVA.

The transition to the Bingham-like behavior may be beneficial for FR properties as it essentially causes physical gelation of a polymer matrix at high temperatures, reducing the spreading of fire through dripping of polymer melts. Thus, the rheological behavior observed in Cu-modified systems is preferred to that observed in Fe-based systems. However, the overall FR performance will depend on the whole spectrum of physico-chemical properties of tested composites rather than the rheological response alone.

3.5. Thermal stability evaluation by TGA

In our previous study [14], the modification of TMI significantly increases the thermal stability of organoclays, i.e., the onset temperature of thermal degradation (in the region of 260–360 °C) shifts towards a higher value (by ca. 30 °C) and the content of solid residue increases substantially. TGA thermograms (in accumulative and derivative modes) of nanocomposites containing unmodified C20A and TMI-modified C20A are illustrated in Fig. 9. It is seen that all nanocomposites exhibited a similar two-stage weight loss behavior. In the first stage of degradation, only a moderate improvement in thermal stability was found in nanocomposites. For example, the onset temperature of degradation (between 260 and 360 °C) for EVA/TMI-modified nanocomposites increased by about 15 °C when compared to pure EVA. Even the organic content did not change much after the first stage of degradation; the formation of char significantly increased with the presence of TMI in the second stage of degradation. It is interesting to note that the maximum amount of char was formed when Cu was used in modification of C20A, while Fe-modified C20A produced char weighing less than that from Cu-modified C20A (Fig. 9a). In addition, the presence of Cu-modified C20A in nanocomposites resulted in the highest content of non-volatile residue at temperatures below 800 °C. On the other hand, the nanocomposite with Fe-modified C20A showed the largest shift (about 40 °C) of the onset degradation among all nanocomposites (Fig. 9b). This difference can be attributed to the secondary effect such as the catalytic activity of iron oxide on the combustion process, which will be discussed next.

3.6. Flame retardation test and char formation

The overall content of solid residue after combustion of nanocomposites in air was strongly affected by the TMI modification of organoclay (results are given in Table 4). The solid residue content in Cu-containing systems was higher than that in nanocomposite containing unmodified organoclays. It was interesting to note that the Fe treatment resulted in decreased

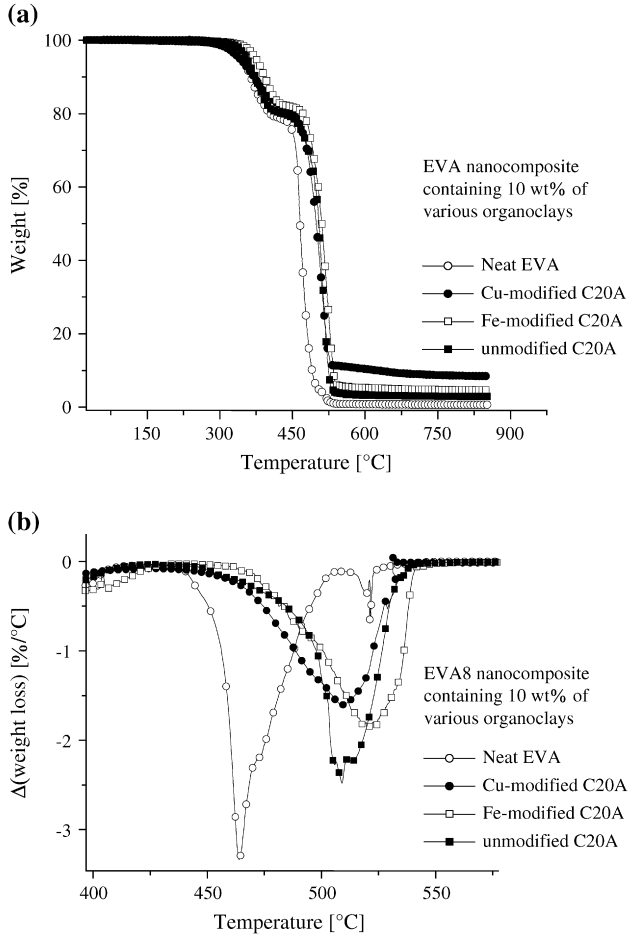

Fig. 9. TGA thermograms for pure EVA, EVA nanocomposites with unmodified and TMI-modified C20A: (a) cumulative weight loss and (b) derivative curves at high temperatures.

solid residue content compared to the Cu-containing system, as well as the nanocomposite containing unmodified organoclays. The observed trends are consistent with the TGA data for nanocomposites in air, however, the exact content of char measured in the combustion test was found to deviate from the values obtained in TGA. It is conceivable that the difference may be due to the effects of heating rate, air humidity and sample shape during the combustion process.

The relationships among the thermal properties, the amount of char formed during combustion of nanocomposites and the corresponding organoclay structure are essential for the mechanism of FR activity. The EVA matrix without C20A burned and dripped, while nanocomposites with C20A and TMI-modified C20A showed visible FR activity, i.e., they formed char upon burning. The FR activity of nanocomposites with TMI-modified C20A was notably better than that of nanocomposites with unmodified C20A. For example, the rates of burning for EVA and three different nanocomposites (with C20A, Cu-modified C20A and Fe-modified C20A) are shown in Table 5. It was found that the rate of burning for the Cu-containing system was significantly reduced when compared with that for the unmodified C20A system (Table 5). Similarly improved FR activity was also found in the Fe-modified system but its effect was lower than that of Cu-modified system.

The SAXS data for the resulting char showed the absence of any scattering maxima (Fig. 10a), suggesting that periodicity in organoclay stacks was completely lost during combustion. On the other hand, WAXD results revealed distinct peaks from the clay structure (Fig. 10b), indicating that the structure of montmorillonite clay mineral persisted in the combustion process. No graphite peaks were observed in WAXD traces of char samples, suggesting the amorphous nature of char formation.

Based on the literature data, the mechanism of thermal degradation for EVA involves two major steps [25,26]: (1) the loss of vinyl acetate units via a de-acylation process resulting in the formation of double bonds and (2) the degradation of resulting unsaturated material. It is conceivable that the presence of TMI-modified organoclays in the EVA matrix may promote crosslinking of unsaturated products formed during degradation, thus hindering the decomposition process. However, the Lewis acidity of clay surface in the presence of TMI may also facilitate the chain scission in EVA. As evidenced from TGA results, the content of char formed in the presence of Cu was substantially more than that in the presence of Fe. It is conceivable that in Cu-modified organoclays, Cu does not promote the combustion reaction. Instead, it forms a complex with the surfactant and results in more charring. However, the increase in the Fe content in the interlayer space may promote both charring and combustion, which would affect the FR activity in an opposite way. The nanocomposite with Fe-modified C20A showed the largest shift in the onset degradation temperature (Fig. 9b) and the resulting char content was less than the nanocomposites containing Cu-modified C20A. The SAXS results indicate that the extent of intercalation is similar in nanocomposites of Fe-modified and Cu-modified organoclays, so EVA chains should have similar access to the active

Table 4
Content of char in nanocomposites determined from the combustion test in air

Organoclays in EVA nanocomposites	Weight of char (%)
C20A (5 wt%)	19.4
C20A (10 wt%)	34.2
C20A (20 wt%)	42.8
Washed C20A (20 wt%)	26.2
Cu-modified C20A (5 wt%)	35.1
Cu-modified C20A (10 wt%)	44.1
Cu-modified C20A (20 wt%)	57.7
Fe-modified C20A (10 wt%)	21.8
Fe-modified C20A (20 wt%)	32.4

Table 5
Rate of burning in various EVA nanocomposites containing unmodified C20A and TMI-modified C20A

Sample	Time (s)	Rate of burning (10^{-2} cm s^{-1})	% Char formed
Neat EVA	55	18.18	0
EVA with C20A (20 wt%)	102	9.80	42.80
EVA with Cu-modified C20A (20 wt%)	146	6.85	57.70
EVA with Fe-modified C20A (20 wt%)	118	8.47	32.4

Ignition time = 5 s, sample length = 10 cm, sample diameter = 1.2 mm.

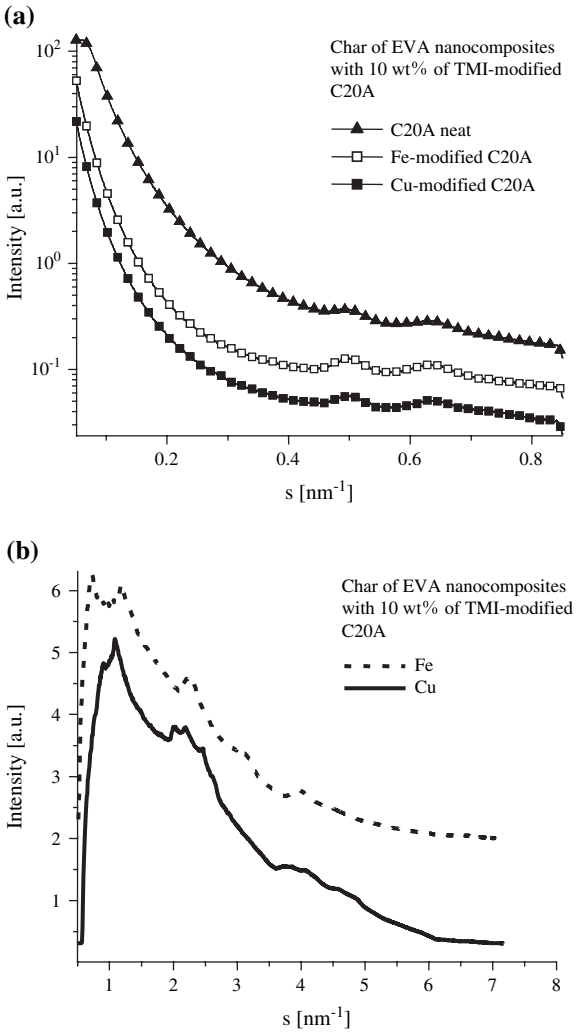

Fig. 10. X-ray characterization of char formed after combustion of various nanocomposites. (a) SAXS profiles and (b) WAXD profiles.

sites on clay surfaces. Thus, the difference in the FR performance may be attributed to the difference in the TMI catalytic reactivity. Since the higher degradation temperature is indicative of greater fire retardation activity, the Fe-modified system may be viewed as more FR than the Cu-modified system, but can result in more enhanced char formation. It is clear that the thorough understanding of the thermal degradation mechanism for polymer nanocomposites is rather complex as this material crosslinks, forms char and degradation of material depends on the absorption characteristic of polymer nanocomposites when exposed to heat sources. While it was shown that the FR activity of organoclays might be improved by the presence of TMI, further research will be needed to elucidate the heat absorption characteristic of polymer nanocomposites in the presence of various TMI and the physical mechanism responsible for thermal degradation.

4. Conclusions

Results in this study indicate that organoclays modified by transition metal ions (TMI) may be used as effective fire retardant (FR) agents for thermoplastic polymers to form nanocomposites with all expected characteristics and enhanced FR properties. TEM and SAXS results indicate that TMI-modified organoclays exhibited strong pillaring effects, which decreased the interlayer *d*-spacing. However, the shearing force during melt mixing could overcome the pillaring effect of TMI such that polymer chains would penetrate the TMI-modified organoclay stacks. Polymer nanocomposites containing TMI-modified organoclays were found to possess higher thermal stability than their counterparts containing unmodified organoclays. It is interesting to note that the effect of TMI on the thermal stability of nanocomposites was not always in accordance with their influence on corresponding organoclays (i.e., more stable clay always forms more stable nanocomposites). For example, while the $CuCl_2$ treatment greatly increased the thermal stability of organoclay, the $FeCl_3$ treated system showed a greater shift of thermal degradation temperature towards higher values. The physico-chemical mechanism behind these phenomena is not yet completely understood. We hypothesize that crosslinking of non-saturated products of thermal degradation, as well as oxidative dehydrogenation processes that would result in aromatization, may be catalyzed by TMI. The catalytic effect may play a role in the increased thermal stability of nanocomposites. Further work is necessary to elucidate the influence of TMI modification on the products of thermal degradation using chromatographic (GC/MC) techniques and on the optimization of catalytic properties of TMI modifiers. It should be noted that nanocomposites containing catalytically active organoclays might also find their use in a handful of applications other than making FR materials.

Acknowledgements

This study was supported by the NSF Inter-American Grant (DMR0302809), NSF MRSEC (DMR 0080604), DOE Grant no. DE-FG02-03ER 15477 and NIST (DMR9984102) at Stony Brook. The SAXS synchrotron beamline X27C was supported by the Department of Energy (Grant no. DE-FG02-99ER 45760).

References

[1] Giannelis EP, Krishnamoorti R, Manias E. Adv Polym Sci 1999;138:107.
[2] Alexandre M, Dubois P. Mater Sci Eng 2000;28:1.
[3] Horrocks AR. In: Price D, editor. Fire retardant materials. Cambridge: Woodhead; 2001.
[4] Gilman JW, Kashiwagi T, Lomakin S, Giannelis E, Manias E, Lichtenhan J, et al. Cambridge: The Royal Society of Chemistry; 1998. p. 203.
[5] Gilman JW, Jackson CL, Morgan AB, Harris R, Manias E, Giannelis EP, et al. Chem Mater 2000;12:1866.
[6] Cornelis A, Laszlo P. NATO ASI Ser Ser C Math Phys Sci 1986;165:213.
[7] LeBaron PC, Wang Z, Pinnavaia TJ. Appl Clay Sci 1999;15:11.
[8] Thomas JM, Adams JM, Graham SH, Tennakoon TB. Chemical conversion using sheet-silicate intercalates. In: Goodenough JB, Whittingham MS, editors. Solid state chemistry of energy conversion and storage, vol. 163. Washington DC: ACS; 1977. p. 298.

[9] Thomas JM. Sheet silicate intercalates: new agents for unusual chemical conversions. In: Whittingham MS, Jacobson AJ, editors. Intercalation chemistry, vol. 1. NY: Academic Press; 1982. p. 55.
[10] Pinnavaia TJ. Science 1983;220:365.
[11] Pinnavaia TJ, Tzou M-S, Landau SD. J Am Chem Soc 1985;107: 4783.
[12] Lewin Menachem, Endo Makoto. Polym Adv Technol 2001;12:215.
[13] Weil ED, Patel NG. Polym Degrad Stab 2003;82:291.
[14] Nawani P, Gelfer MY, Hsiao BS, Frenkel A, Gilman JW, Khalid S, submitted for publication.
[15] Beyer Günter. Fire Mater 2001;25(5):193.
[16] Beyer G. Fire Mater 2005;29:61.
[17] Peeterbroeck S, Alexandre M, Nagy JB, Pirlot C, Fonseca A, Moreau N, et al. Compos Sci Technol 2004;64:2317.
[18] Xie W, Gao ZM, Pan WP, Hunter D, Singh A, Vaia R. Chem Mater 2001;13:2979.
[19] Gelfer MY, Burger C, Chu B, Hsiao BS, Drozdov AD, Si M, et al. Macromolecules 2005;38(9):3765.
[20] Starnes WH, Pike RD, Cole JR, Doyal AS, Kimlin EJ, Lee JT, et al. Polym Degrad Stab 2003;82:15.
[21] Bom D, Andrews R, Jacques D, Anthony J, Chen B, Meier MS, et al. Nano Lett 2002;2(6):615.
[22] UL 94. Test for flammability of plastic materials for parts in devices and appliances; 2000.
[23] Gelfer M, Burger C, Fadeev A, Sics I, Chu B, Hsiao BS, et al. Langmuir 2004;20:3746.
[24] Gelfer MY, Song HH, Liu L, Avila-Orta C, Yang L, Si M, et al. Polym Eng Sci 2002;42:1841.
[25] Troitskii BB, Razuvayev GA, Khokhlova LV, Bortnikov GN. J Polym Sci Poly Symp 1973;42:1363.
[26] Zanetti M, Camino G, Thomann R, Mülhaupt R. Polymer 2001;42: 4501.